Idealized Hot Spot Experiments with a General Circulation Model

ERIC D. MALONEY

College of Oceanic and Atmospheric Sciences, Oregon State University, Corvallis, Oregon

ADAM H. SOBEL

Department of Applied Physics and Applied Mathematics, and Department of Earth and Environmental Sciences, Columbia University, New York, New York

(Manuscript received 15 March 2006, in final form 8 August 2006)

ABSTRACT

Idealized experiments are conducted using a GCM coupled to a 20-m slab ocean model to examine the short-term response to an initial localized positive equatorial SST anomaly, or "hot spot." A hot spot is imposed upon an aquaplanet with globally uniform 28°C SST, insolation, and trace gas concentrations designed to mimic tropical warm pool conditions. No boundary condition or external parameter other than the Coriolis parameter varies with latitude. A 15-member ensemble is initiated using random atmospheric initial conditions. A 2°C equatorial warm anomaly is switched on, along with ocean coupling (day 0).

Enhanced deep convection rapidly develops near the hot spot, forcing an anomalous large-scale circulation that resembles the linear response of a dry atmosphere to a localized heating, as in the Gill model. Enhanced convection, the anomalous large-scale circulation, and enhanced wind speed peak in amplitude at about day 15. Enhanced latent heat fluxes driven primarily by an increase in vector mean wind damp the anomalous heat content of the ocean near the hot spot before day 20. Between day 20 and day 50, suppressed latent heat fluxes due to suppressed synoptic eddy variance cause a warming of the remote Tropics in regions of anomalous low-level easterly flow. This wind-driven evaporative atmosphere–ocean exchange results in a 60–70-day oscillation in tropical mean oceanic heat content, accompanied by a compensating out-of-phase oscillation in vertically integrated atmospheric moist static energy. Beyond day 70 of the simulation, positive SST anomalies are found across much of the tropical belt. These slowly decay toward the 28°C background state.

1. Introduction

Determining what limits tropical sea surface temperatures (SSTs) has been a topic of intense research over the last couple of decades. Key questions include the extent to which SST regulation is governed by local (e.g., Ramanathan and Collins 1991; Sud et al. 1999) versus large-scale (e.g., Wallace 1992; Waliser and Graham 1993; Hartmann and Michelsen 1993; Lau et al. 1994; Pierrehumbert 1995; Larson et al. 1999) processes, as well as the relative roles of evaporative-driven (e.g., Wallace 1992; Hartmann and Michelsen 1993) versus radiative-driven (e.g., Zhang and McPhaden 1995) regulation of tropical SST. Ocean dynamics also appear to play a significant role in tropical SST regulation (e.g., Waliser 1996; Clement et al. 1996; Sun and Liu 1996; Anderson et al. 1996; Ralph et al. 1997; Seager and Murtugudde 1997; Clement et al. 2005).

This study focuses on the short-term regulation of SST associated with localized positive tropical SST anomalies, or "hot spots." Waliser (1996) defined a hot spot as a region of greater than 1×10^6 km^2 area in which SST exceeds 29.75°C for at least one month. These hot spots generally form in warm pool regions of the Tropics during periods of suppressed evaporative and enhanced downward shortwave fluxes, conditions consistent with the convectively suppressed phase of the tropical intraseasonal oscillation (ISO; Madden and Julian 2005). These convectively suppressed periods are also characterized by low surface salinity and minimal turbulent mixing, conditions that favor shallow mixed layers and thus aid in rapid warming of SST (e.g., Lukas

Corresponding author address: Eric D. Maloney, College of Oceanic and Atmospheric Sciences, Oregon State University, 104 COAS Admin. Building, Corvallis, OR 97331-5503.
E-mail: maloney@coas.oregonstate.edu

DOI: 10.1175/JCLI4053.1

and Lindstrom 1991; Anderson et al. 1996). Strong ISO events can generate oceanic hot spots of amplitude exceeding 1°C (Weller and Anderson 1996).

Large-scale dynamical disturbances such as the ISO appear to be important not only for generating oceanic hot spots but also for removing such SST anomalies on short-time scales (e.g., Waliser and Graham 1993). To the extent that both the generation and termination of hot spots are forced by the ISO, and that the ISO can be thought of as a primarily atmospheric phenomenon, which would exist in some form without ocean coupling (as suggested by GCM experiments, e.g., Zhang et al. 2006), hot spots may simply be thought of as the positive anomaly phase of the SST response to the ISO, rather than a distinct phenomenon. Nonetheless, Sobel and Gildor (2003, hereafter SG03) showed that a simple single-column model could sustain unforced free oscillations with periods in the intraseasonal range. The mechanism responsible for the oscillation resembles that identified observationally by Waliser (1996): a period of suppressed convection allows the SST to warm due to suppressed latent heat fluxes and increased surface shortwave radiation, but the positive SST anomaly that develops eventually destabilizes the atmosphere to convection, which leads to reduced shortwave and enhanced latent heat fluxes, reversing the cycle. This suggests that coupled feedbacks at a single location, independent of a propagating ISO, could in principle generate SST variability of the sort associated with hot spots. In reality, since the ISO exists and its period is close to that of the free single-column oscillations, the two phenomena can be expected to couple closely. This means that the SST variability associated with hot spots, besides being generated by the atmosphere, may feed back to modulate the strength of the ISO (e.g., Wang and Xie 1998; Waliser et al. 1999; SG03; Maloney and Sobel 2004).

We examine the short-term response of the climate system to the imposition of a 2°C equatorial SST hot spot in an atmospheric general circulation model (GCM) coupled to a simple slab ocean model (SOM). Although motivated by our interest in tropical intraseasonal variability, our simulations can also be thought of simply as basic numerical experiments in moist climate dynamics. Our experiment is highly idealized in that we superimpose the hot spot on a basic state of globally uniform 28°C SST. This highly idealized framework allows us to examine the short-term response to the hot spot with minimal interference from inhomogeneity that may complicate the interpretation. Our study neglects ocean dynamical processes, such as mixed layer deepening by turbulent entrainment during periods of high wind, which may regulate the short-term response of the climate system to imposition of an SST anomaly (e.g., Anderson et al. 1996). However, a SOM may be adequate to represent the role of ocean coupling on atmospheric intraseasonal variability (as is often assumed; see, e.g., Shinoda and Hendon 1998; Kessler 2005).

The most relevant recent studies to ours are the idealized simulations conducted by Hosaka et al. (1998), Neale and Hoskins (2000a,b), and Nakajima et al. (2004). In these studies, a temporally invariant equatorial SST hot spot was imposed on a zonally symmetric background SST distribution using an aquaplanet atmospheric GCM. The transient and steady atmospheric responses to the hot spot were examined. Our study builds on this work in that coupling to a simple ocean allows SST to evolve after imposition of the hot spot. Our globally uniform background SST distribution is also different than that used in these previous studies, which contained latitudinal gradients of SST in both the Tropics and extratropics. The lack of extratropical SST gradients here reduces internal atmospheric variability, allowing greater significance in the forced response with smaller ensembles.

Our paper is organized as follows. Section 2 describes our idealized aquaplanet experiment with a 20-m depth SOM in which a 2°C hot spot is imposed on a globally uniform 28°C SST background state. Section 3 describes the atmospheric response after switch-on of the hot spot. Section 4 describes the heat budget of the coupled ocean–atmosphere response. Section 5 analyzes the evolution of latent heat flux. Hot spot experiments detailing sensitivity to SOM depth and a realistic background distribution of SST and continents are described in section 6. Section 7 presents a discussion and conclusions.

2. Model and experiment design

a. The NCAR CAM2.0.1

We use a modified version of the National Center for Atmospheric Research (NCAR) Community Atmosphere Model Version 2.0.1 (CAM2; Kiehl and Gent 2004). The version of CAM2 that we use includes a parameterization of deep convection developed by Moorthi and Suarez (1992; relaxed Arakawa–Schubert) in place of the standard CAM2 deep convection parameterization of Zhang and McFarlane (1995). The relaxed Arakawa–Schubert parameterization has been documented to produce superior tropical intraseasonal variability to the Zhang and McFarlane (1995) scheme in this model (e.g., Maloney and Hartmann 2001) and may thus provide a more realistic transient response to the imposition of a hot spot. The configuration of

CAM2 we use here is identical to that used in Maloney and Sobel (2004) to test the sensitivity of the model ISO to ocean mixed layer depth.

Our CAM2 simulations are conducted at T42 horizontal resolution, which approximately corresponds to a grid resolution of 2.8° latitude by 2.8° longitude. Twenty-six levels in the vertical are resolved, and the model time step is 20 min.

b. Slab ocean model

To conduct our transient hot spot experiments, we use a simple SOM based on the formulation of Hansen et al. (1984):

$$\rho_o C_o h \frac{\partial T}{\partial t} = F + Q, \tag{1}$$

where ρ_o is density, C_o is the heat capacity of seawater, h is the mixed layer depth, T is the temperature of the mixed layer, F is the net surface heat flux into the ocean (radiative, sensible, and latent), and Q is the net oceanic heat transport into the mixed layer. Here Q is calculated using climatological surface fluxes from a prescribed SST control simulation as the oceanic transport required to close the mixed layer heat budget (1). The design of the SOM ensures that the SST climatology of the coupled experiments reproduces the climatology of the prescribed-SST control experiment.

c. The aquaplanet 28°C control simulation

Our tropical hot spot experiment is conducted in a highly idealized framework. We describe here the 15-yr control simulation of CAM2 that was used to provide the climatology and Q flux for the idealized coupled hot spot experiment. The control simulation (and subsequent hot spot experiment) is forced with globally uniform conditions mimicking those in the west Pacific warm pool. The model is run as an aquaplanet with SST fixed at a globally invariant 28°C. A temporally and globally uniform insolation of 400 W m^{-2} was applied using a zenith angle of 0° (no diurnal cycle). The concentrations of ozone and other trace gases (other than water vapor) are globally invariant and prescribed to have a tropical average profile. No boundary condition or external parameter other than the Coriolis parameter varies in latitude. This uniform forcing produces a top-of-atmosphere radiative energy balance everywhere on the globe that is characteristic of observed tropical warm pool conditions.

The climatology of surface wind components and precipitation from the 28°C control simulation is shown in Fig. 1. The atmosphere is close to a state of uniform radiative-convective equilibrium, with zero large-scale

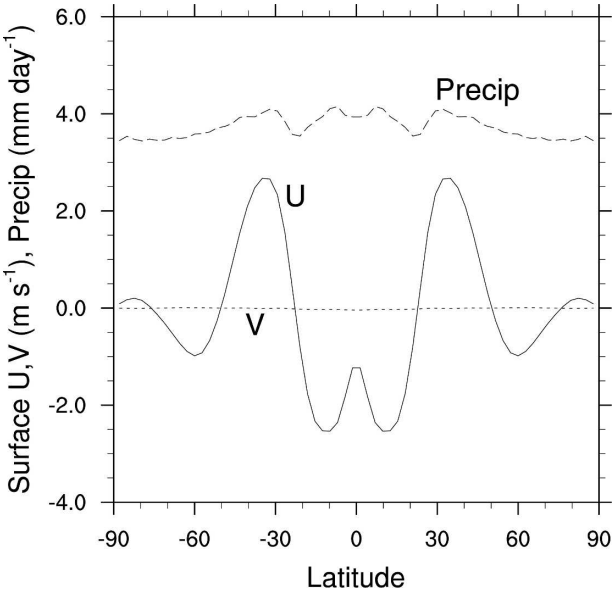

FIG. 1. Climatological surface wind components and precipitation as a function of latitude for the 28°C control simulation.

circulation and uniform precipitation. This state is not quite attained, as a large-scale circulation is apparently induced by meridional variations in the Coriolis parameter. Weak zonally symmetric circulations that resemble Hadley cells exist in the mean. Weak midlatitude surface westerlies and weak tropical trade winds are produced in the model. Tropical precipitation exhibits very weak local maxima of about 4 mm day^{-1} centered near 10°S and 10°N. A second pair of precipitation maxima are centered near 30°N and 30°S latitude. These results bear some resemblance to those of Kirtman and Schneider (2000), who also simulated a spontaneously generated large-scale circulation in an aquaplanet AGCM experiment with globally uniform forcing. The latitudinal variability in both zonal mean precipitation and meridional wind (i.e., the Hadley circulation) is much weaker in our experiments than in theirs. Our mean surface zonal winds, on the other hand, are stronger than theirs. The strength of these zonal winds in the almost complete absence of a zonal mean overturning circulation likely means that the surface zonal winds are eddy driven, though we have not analyzed the zonal momentum budget to determine this.

It is possible that the precipitation and wind climatologies of our model may be sensitive to the value of the globally uniform SST. Barsugli et al. (2005) conducted idealized AGCM experiments with different values of globally uniform SST (20°, 25°, and 30°C) and found high sensitivity in the structure and amplitude of the ITCZ. Barsugli et al. (2005) could create stronger

equatorial precipitation maxima than found in our Fig. 1 by setting the value of SST to 20° or 30°C. We will show below that the hot spot response in our model is regulated in part by the interaction of the anomalous flow field with the basic-state wind. Thus, we cannot rule out that the response would be sensitive to a different background SST than 28°C. However, as we will describe below in the context of experiments with realistic February SST, radiative forcing, and continents, the response to the hot spot appears to be at least qualitatively similar when using a more realistic basic state.

d. Aquaplanet hot spot experiment

Our hot spot experiment simulates the coupled response to the instantaneous imposition of a 2°C equatorial anomaly on an idealized 28°C background state. Since substantial subseasonal variability is characteristic of the GCM we use, 15-member ensembles are generated for each hot spot experiment. These use random initial conditions from the 28°C control simulation to produce a statistically robust result. In reality, tropical hot spots may owe their existence at least in part to intraseasonal oscillations (e.g., Waliser et al. 1999). Thus, observed hot spots may be associated with a more limited set of initial atmospheric states than those that would be generated by a random selection. We use random initial conditions here for simplicity.

Initial conditions for the ensemble members are taken at 1-yr intervals from the 28°C control simulation. For each ensemble member, a spinup period is conducted in which clouds and other physical processes are allowed to adjust while holding SSTs fixed at 28°C. The equatorial SST perturbation and ocean coupling are then switched on, and the coupled model is allowed to freely evolve for 180 days. We refer to the switch-on time as day 0.

We choose a Gaussian form and a spatial scale for the SST perturbations that is based on the observed structure of warm pool hot spots shown in Waliser (1996, his Fig. 5b). Our SST perturbation has the following form:

$$T' = T_o \exp\left[\frac{-(\phi - \phi_o)^2}{(14°)^2}\right] \exp\left[\frac{-(\lambda - \lambda_o)^2}{(20°)^2}\right], \tag{2}$$

where ϕ and λ are latitude and longitude in degrees, respectively, ϕ_o and λ_o are the corresponding center coordinates of the hot spot, and T_o is the amplitude of the SST anomaly. The magnitude of the anomaly drops by a factor of e^{-1} at 14° latitude and 20° longitude away from the center.

We set $\phi_o = 0°$ and $\lambda_o = 180°$, though the longitudinal position of the hot spot is arbitrary since the background state is zonally uniform. Here T_o is set to +2°C (see Fig. 5a), an amplitude that is larger than that typically associated with observed hot spots. This serves to maximize the signal-to-noise ratio of our ensemble-mean response and increase the likelihood of a statistically significant result. SOM depth is set to 20 m, a typical west Pacific warm pool mixed layer depth. Sensitivity of the tropical response to SOM depth is briefly described in section 6.

3. Atmospheric response

We now analyze our idealized 2°C aquaplanet hot spot experiment. Results are presented as the ensemble mean anomaly. Unless otherwise stated, anomalies are calculated as deviations from the climatology of the 15-yr 28°C aquaplanet control simulation. Where statistical significance is noted, ensemble-mean anomalies are determined to be significantly different from zero at the 95% confidence level using the t statistic in conjunction with the 15-member ensemble standard deviation.

Figure 2 describes the evolution of precipitation and surface wind anomalies for the idealized hot spot experiment. Panels display ensemble mean anomalies in 5-day averages starting on the day indicated. Enhanced precipitation develops over the hot spot around day 0 and then reaches its maximum amplitude by about day 10. An anomalous global circulation is generated that resembles the forced response to a steady localized equatorial heat source as described by Gill (1980). Easterly anomalies associated with an anomalous Kelvin wave circulation extend eastward from the hot spot past 360°E. These easterly anomalies have an Ekman component that causes meridional convergence onto the equator. A Rossby wave circulation associated with strong equatorial low-level westerly anomalies is forced to the west of the hot spot. The anomalous circulation reaches maturity near day 10 and gradually weakens thereafter.

The initial response of precipitation and the large-scale circulation to the hot spot resembles the steady response obtained by Hosaka et al. (1998) for a temporally invariant hot spot. Comparing our day-10 response to their steady response, we see a similar enhancement of precipitation near the hot spot, and an additional enhancement of precipitation in a narrow equatorial band to the east of the hot spot. This narrow band of anomalous precipitation is associated with surface easterly anomalies and surface convergence. Hosaka et al. (1998) suggests that this equatorial precipi-

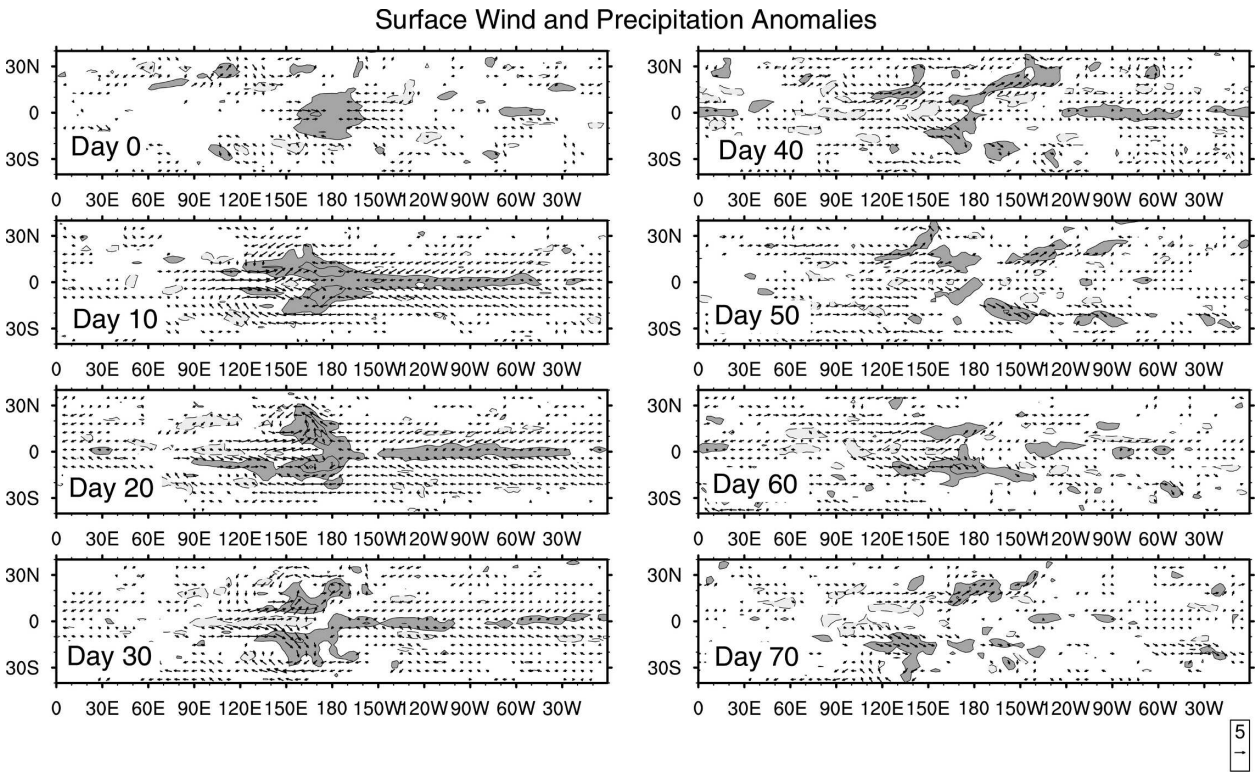

FIG. 2. Ensemble mean surface vector wind and precipitation anomalies as a function of time after imposition of the hot spot. Plotted are 5-day averages starting at the indicated lag. Anomalies are calculated with respect to the 28°C control simulation. The reference vector ($m\ s^{-1}$) is shown at the bottom right. Only vectors statistically significant at the 95% confidence level are shown. The precipitation contour interval is 4 mm day^{-1}, starting at 2 mm day^{-1}. Values greater (less) than 2 mm day^{-1} (-2 mm day^{-1}) are dark (light) shaded. Negative contours are dashed.

tation feature is forced primarily by anomalous frictional convergence. However, this region of easterly anomalies is also accompanied by enhanced surface evaporation at day 10 (Fig. 3). Hosaka et al. (1998) conducted sensitivity experiments in which wind-induced surface heat exchange (WISHE) was removed by setting the surface wind speed in the calculation of surface fluxes to climatology. These experiments suggested that WISHE plays a secondary role to frictional convergence in generation of the equatorial precipitation anomaly. However, previous studies have shown that precipitation in our model is highly sensitive to wind-evaporation feedback (e.g., Maloney and Sobel 2004; Maloney and Esbensen 2005). Not having performed a "no-WISHE" experiment here, we cannot rule out that enhanced evaporation contributes significantly to the anomalous equatorial precipitation band to the east of the hot spot in our model.

A broader examination of latent heat flux anomalies indicates that enhanced evaporation occurs in the vicinity of the hot spot near day 0 (Fig. 3). Positive anomalies in air–sea disequilibrium and wind speed account appear to be about equally important in producing the enhanced latent heat flux in the vicinity of the hot spot near day 0 (not shown here). As the anomalous large-scale circulation fully develops by day 10, positive latent heat flux anomalies extend across much of the Tropics. We will show below that these latent heat flux anomalies are primarily wind induced. Figure 3 also indicates an interesting suppression of latent heat flux in the remote Tropics away from the hot spot after day 20, with the amplitude of these negative anomalies maximizing near day 40. These suppressed fluxes will be shown to be important for redistributing the anomalous heat content in the hot spot region to the remote Tropics. As also explained below, these regions of suppressed latent heat flux are primarily wind induced.

Convective heating near the hot spot forces positive tropospheric temperature anomalies that spread rapidly eastward away from the hot spot between day 0 and day 20 (Fig. 4). This eastward propagation is consistent with the Kelvin wave response typically observed in response to the switch-on of an atmospheric equatorial heat source (e.g., Heckley and Gill 1984; Bantzer and Wallace 1996) and is a mechanism by

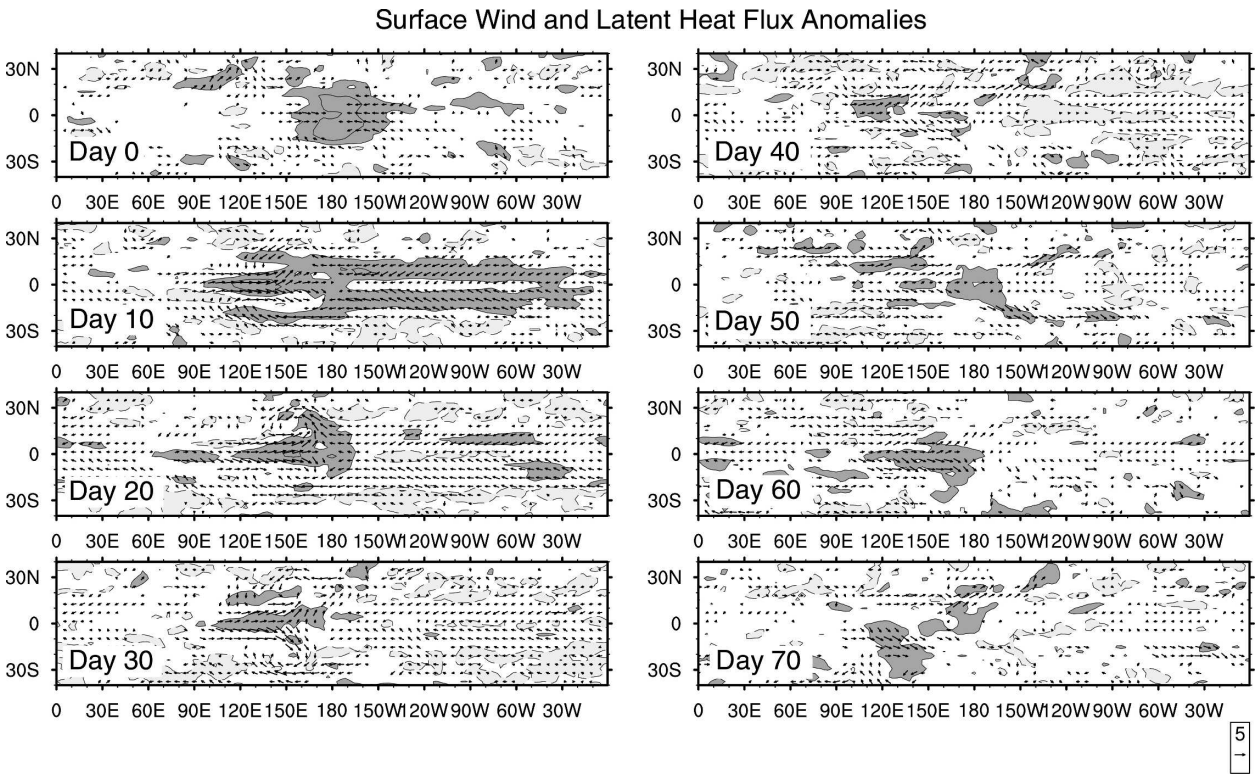

FIG. 3. Same as in Fig. 2, except for surface vector wind and latent heat flux anomalies. The latent heat flux contour interval is 20 W m^{-2}, starting at 10 W m^{-2}. Values greater (less) than 10 W m^{-2} (-10 W m^{-2}) are dark (light) shaded. Negative contours are dashed. Positive values represent a flux of heat out of the ocean.

which the tropical atmosphere quickly removes zonal temperature gradients (e.g., Chiang and Sobel 2002; Su et al. 2005). The temperature front in our model propagates eastward at about 20 m s^{-1} (e.g., cf. the day-0 and -10 temperature anomalies), slower than the 40–50 m s^{-1} propagation speed associated with a free first baroclinic mode Kelvin wave in a dry atmosphere (e.g., Milliff and Madden 1996). The 20 m s^{-1} is consistent with the speed of the temperature front in Nakajima et al. (2004), however. Diabatic heating anomalies are apparently acting to reduce the effective static stability and thus the propagation speed of the gravest baroclinic mode Kelvin wave in our simulations as compared to a dry Kelvin wave, as found in spectral analysis of outgoing longwave observations (Wheeler and Kiladis 1999). We note that the vertically averaged tropospheric temperature anomalies have a substantial zonal mean component (~0.4°C) that peaks shortly after day 20 (not shown here). This warming is consistent with an increase in tropical mean atmospheric moist static energy, as will be shown below. Similar tropical mean warming on subseasonal time scales has been observed to occur in association with the ISO (Bantzer and Wallace 1996), where individual events can warm equatorial mean tropospheric temperatures by up to 0.5°C. Peak warming occurs about 15 days after the initiation of ISO convection in the Indian Ocean. Tropospheric warm anomalies in our model rapidly decay after day 30. The evolution of tropospheric temperature forms one component of the cycling of heat between the atmosphere and ocean that characterizes the transient response to the hot spot.

4. Heat budget

The evolution of ensemble mean SST anomalies is displayed in Fig. 5. Day 0 shows the hot spot in its near-initial form. Anomalies at the original location of the hot spot monotonically decrease in amplitude throughout the duration of the simulations. A modest initial cooling of the remote Tropics occurs until about day 20 (we refer to the remote Tropics as everything outside of the 150°–210°E band). The remote Tropics warm significantly after day 20, particularly within 180° longitude to the east of the hot spot. Warm SST anomalies reach maturity by about day 50. Thus, by day 50 of the simulation, the atmosphere has acted to redistribute much of the heat content anomaly contained within the

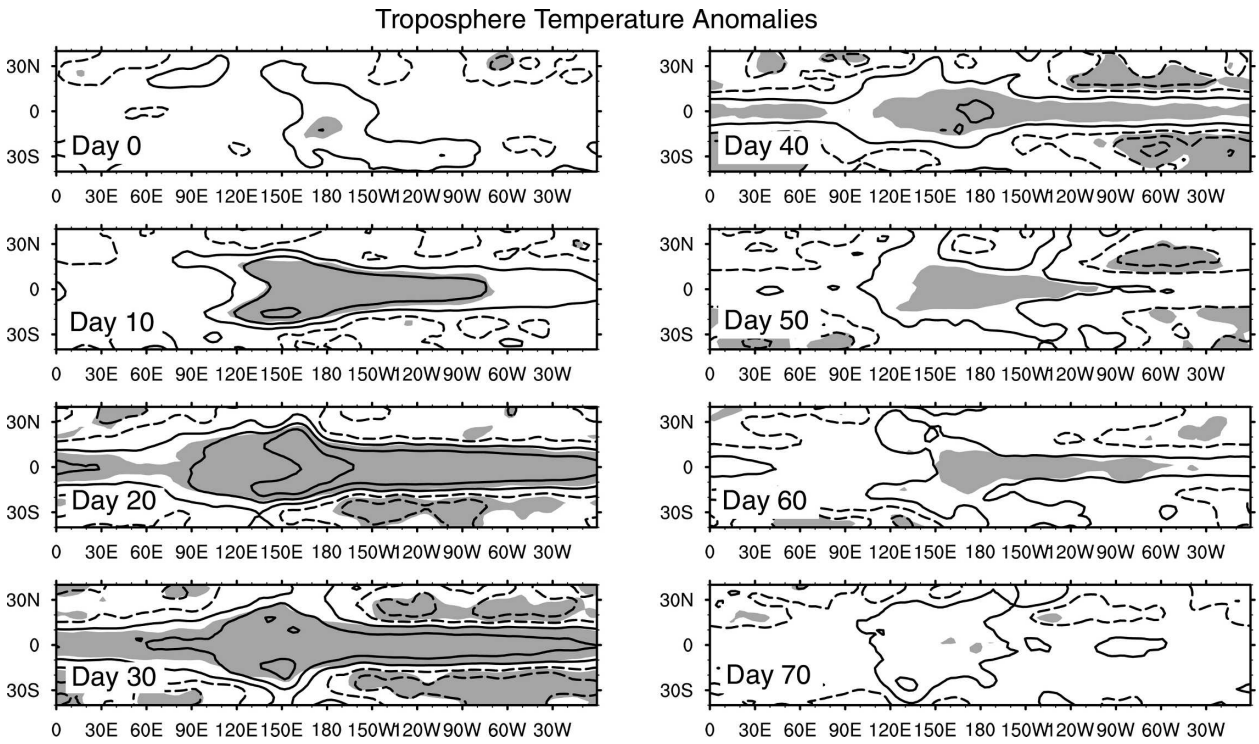

FIG. 4. Same as in Fig. 2, except for vertically averaged tropospheric temperature anomalies. The temperature contour interval is 0.4 K, starting at 0.2 K. Shading represents regions significantly different from zero at the 95% confidence interval.

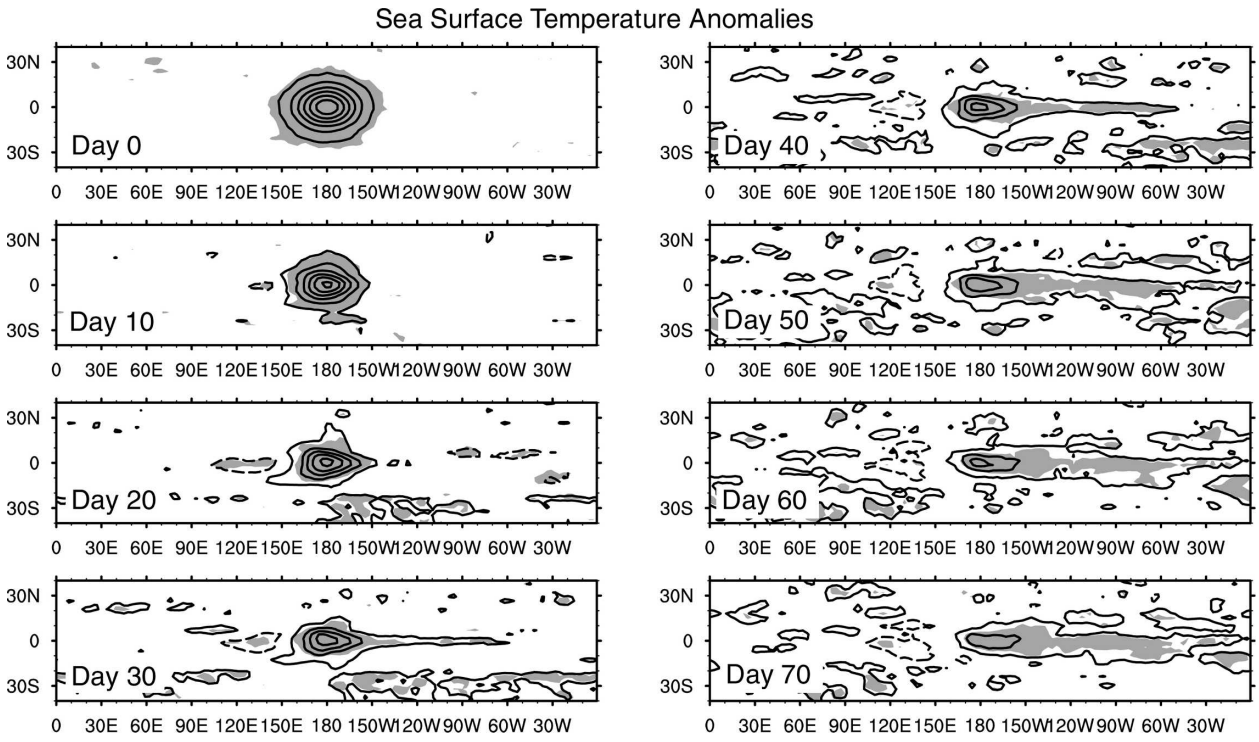

FIG. 5. Same as in Fig. 2, except for sea surface temperature anomalies. The temperature contour interval is 0.3 K, starting at 0.15 K. Shading represents regions significantly different from zero at the 95% confidence interval.

original hot spot to the remote Tropics. Beyond day 70 (not shown here), the pattern of SST anomalies remains relatively invariant, although the amplitude of the anomalies gradually decays with time.

We analyze the evolution of tropical mean (30°N–30°S, 0°–360°E averaged) ocean heat content anomalies for a more quantitative view of the tropical ocean heat budget (Fig. 6a). Interestingly, the transient tropical mean response to the hot spot appears to be an oscillation in oceanic heat content with a time scale of about 60–70 days. Heat is removed from the tropical ocean until day 20. The tropical ocean gains heat after day 20 until a maximum in tropical ocean heat content occurs around day 45. The anomalous heat content of the ocean at day 45 is greater than that imposed in the initial hot spot anomaly. After day 45, oceanic heat content anomalies are damped.

Confidence intervals in Fig. 6a indicate that a statistically significant oscillation in tropical oceanic heat content occurs after imposition of the hot spot, with a time scale of about 60–70 days. It is interesting that this time scale is at the upper limit of that associated with the ISO. While the response of the atmosphere–ocean system to the hot spot in many ways does not resemble the eastward-propagating ISO, the zonal mean response to the hot spot does appear to mimic in some respects the zonal mean behavior of the ISO (e.g., tropospheric temperature; Bantzer and Wallace 1996).

We separately examine ensemble-mean ocean heat content anomalies (a) in the vicinity of the hot spot (30°N–30°S, 150°–210°E) and (b) in the remote Tropics (the rest of the 30°N–30°S band) in Fig. 6b. Heat content anomalies in the vicinity of the original hot spot simply dampen in time. Conversely, the anomalous heat content of the remote Tropics is relatively negligible until about day 20, when it rapidly increases to reach a maximum near days 40–50. After day 50, the heat content anomalies of the remote Tropics slowly damp toward zero. The net effect of the cooling in the immediate vicinity of the hot spot and the rapid heating of the remote tropical oceans after day 20 is the apparent oscillation in tropical ocean heat content.

The decay of SST anomalies in the vicinity of the hot spot suggests that the GCM does not support local unforced intraseasonal oscillations in SST and precipitation. In the idealized model of SG03, such unforced oscillations did occur for certain values of the model parameters, namely, small convective adjustment time and large values of a parameter expressing the ratio of radiative or surface heat flux anomalies to convective latent heating anomalies. A rough approximation to the stability criterion of SG03, which we do not expect to apply exactly here in any case due to the much greater

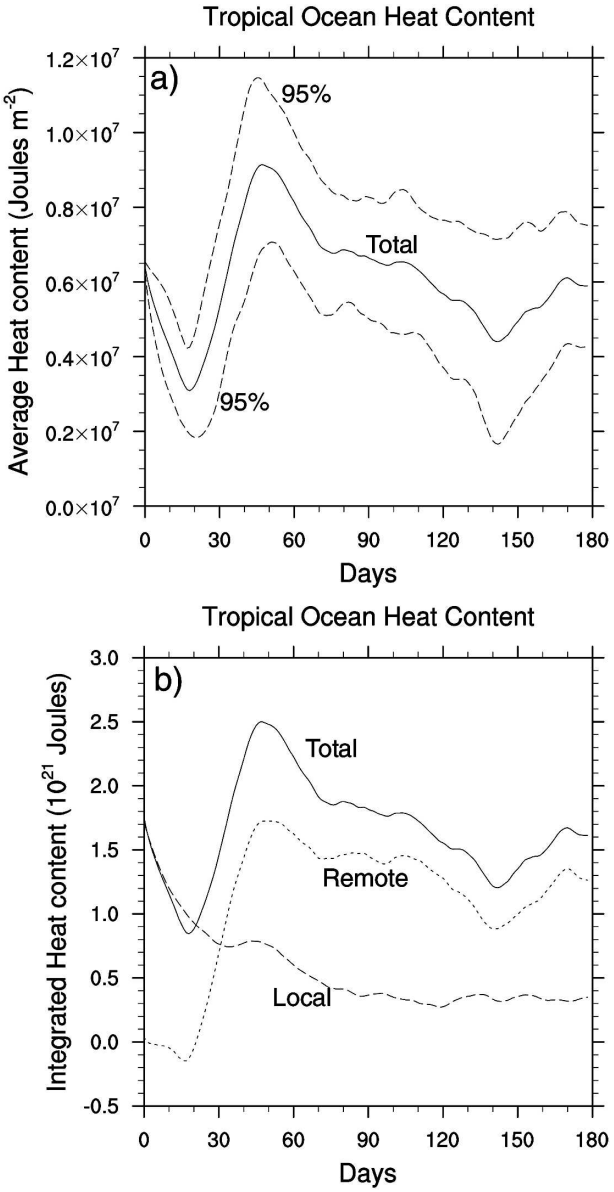

FIG. 6. Ensemble mean (a) 30°N–30°S, 0°–360°E averaged tropical oceanic heat content as a function of time after imposition of the hot spot. (b) Spatially integrated oceanic heat content for the entire Tropics (30°N–30°S, 0°–360°E), the region in the vicinity of the hot spot (30°N–30°S, 150°–210°E), and the remote Tropics (the 30°N–30°S band excluding the hot spot vicinity). (a) Includes 95% confidence intervals on the ensemble mean heat content, calculated using the *t* statistic.

complexity of the model used for the present simulations, is that growth of precipitation anomalies and local unforced oscillations can be supported if moist static energy (MSE) generation by reduced longwave cooling and surface fluxes exceeds MSE export through divergent circulations, resulting in a negative "effective gross moist stability" (Su and Neelin 2002; Bretherton and

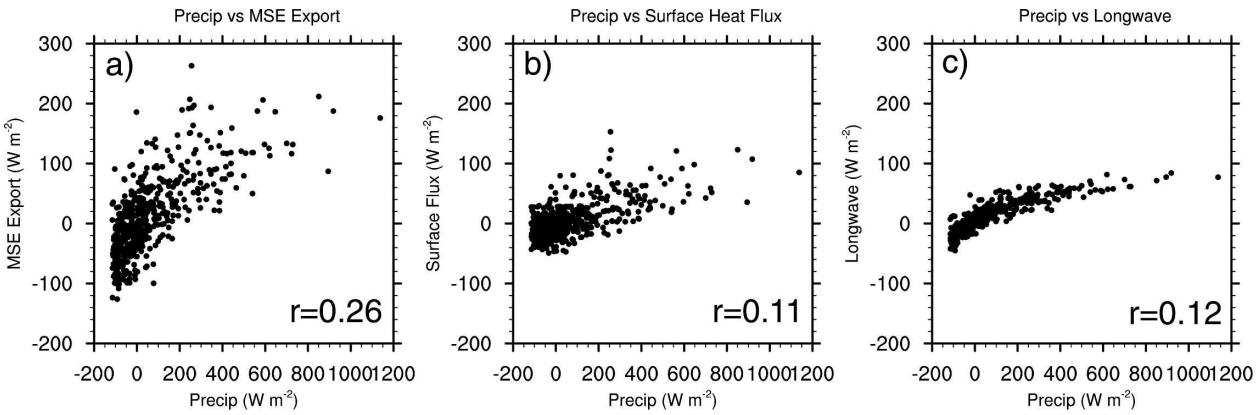

FIG. 7. Scatterplots of (a) vertically averaged MSE export, (b) net surface heat flux, and (c) surface minus top-of-atmosphere longwave flux vs precipitation. The regression coefficient is shown at the bottom right of each plot.

Sobel 2002; Sobel et al. 2004). Regression coefficients derived from scatterplots are used to diagnose the MSE budget in the vicinity of the hot spot (Fig. 7). Vertically averaged MSE export, net surface heat flux, and surface minus top-of-atmosphere longwave flux are plotted versus precipitation. The export term was computed as a residual in the MSE budget. Each point represents a 5-day average for an ensemble member over an 8° × 8° box centered at 10°S, 174°E, where the strongest area-averaged precipitation anomalies occur (Fig. 2). The regression coefficients for surface flux and longwave heating are 0.11 and 0.12, respectively, while that for export is 0.26. Thus, MSE export slightly exceeds generation by surface fluxes and longwave radiative heating, and local instability is not supported; the observed stability of the hot spot to free oscillations appears to be consistent with what theory would predict, given the parameters diagnosed from the simulation's MSE budget. Results are not sensitive to the box location.

The ratio of moist static energy export to dry static energy transport near the hot spot, which can be thought of as a normalized gross moist stability, is 0.23. This ratio is higher than the 0.14 used in SG03, which is also expected to have a stabilizing effect. The gross moist stability is sensitive to the moist static energy and large-scale vertical motion profiles. These in turn are sensitive to model physics, so changes to the model physics could lead to local instability in the sense of SG03. Modest increases in wind evaporation feedback, for example, through a convective gustiness parameterization (Bretherton et al. 2005) or a different basic-state wind field, could also lead to instability, as could stronger cloud–radiation feedbacks.

Unlike the damping of ocean heat content anomalies in the vicinity of the hot spot, out-of-phase oscillations occur in tropical integrated oceanic heat content and atmospheric MSE, shown in Fig. 8 relative to their respective values at day 0. Because fluid motions in the model atmosphere allow efficient transport across latitudes unlike in the slab ocean model, ocean–atmosphere heat exchange that occurs within a given latitude band may be manifest in atmospheric moist static energy anomalies at an expanded range of latitudes. We therefore integrate over 30°N–30°S for the ocean and a wider, but somewhat arbitrary, 40°N–40°S band for the atmosphere. The cancellation of atmospheric and ocean heat content anomalies for these two

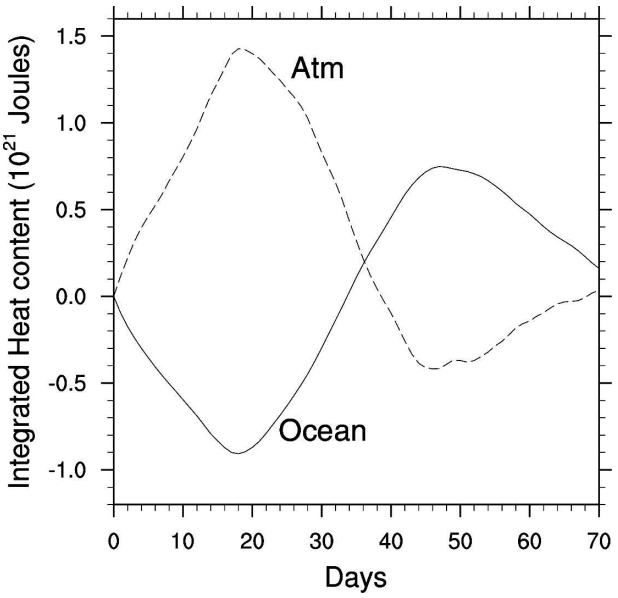

FIG. 8. Ensemble mean tropical integrated oceanic heat content (30°N–30°S, 0°–360°E) and vertically integrated moist static energy (40°N–40°S, 0°–360°E) as a function of time after imposition of the hot spot. Anomalies are calculated relative to the respective ocean and atmosphere heat contents just after imposition of the hot spot.

different bands is more complete than when using a common 30°N–30°S band. Vertically integrated atmospheric MSE peaks near day 20 (Fig. 8), consistent with the maximum in zonal mean tropospheric temperature observed at that time (Fig. 4). Day 20 is also near the local minimum in ocean heat content. A relative minimum in atmospheric MSE occurs about day 50, when tropical ocean heat content is anomalously high.

We now examine the mechanisms that regulate ocean and atmosphere heat content and the exchange of energy between the two reservoirs after imposition of the hot spot. To do this, we will first analyze the evolution of tropical mean surface heat and radiative flux anomalies (Fig. 9). A net flux from the ocean to atmosphere is defined as positive.

Latent heat flux dominates the response to the hot spot in the first 50 days of the simulation and thus regulates the transient oscillatory response to the hot spot. Latent heat flux dominates the response in both the vicinity of the hot spot and in the remote Tropics (not shown here). Evaporative fluxes are anomalously strong before day 20, with the strongest latent heat flux anomalies (4 W m^{-2} in the tropical average) occurring near day 15. Suppressed latent heat fluxes ensue after day 20, reaching a tropical mean minimum of about -3 W m^{-2} near day 35. Tropical mean latent heat flux anomalies are generally smaller after day 50 of the simulation, although they are highly variable in time. The standard deviation of latent heat flux anomalies among ensemble members is also generally high from day 50 onward (implied by Fig. 6a). Tropical mean shortwave anomalies are relatively modest compared to latent heat flux anomalies, with an enhanced shortwave flux into the ocean at day 15 (~ -2 W m^{-2}) that opposes the extraction of heat by latent heat fluxes. These shortwave anomalies are due primarily to suppression of convection in the remote Tropics. Net surface shortwave anomalies in the vicinity of the hot spot at day 15 are positive (not shown here), indicating a reduced flux of radiation into the ocean caused by enhanced convection. A related relationship between the local and remote tropical shortwave budget was suggested by Zhang et al. (1996) in association with El Niño–Southern Oscillation warm anomalies. Sensible heat and longwave radiative flux anomalies are generally modest during the first 50 days of the simulation, although we note that tropical mean longwave flux anomalies are consistently elevated at about 1 W m^{-2} after day 50. This enhanced longwave flux from the surface likely plays an important role in the gradual weakening of the warm SST anomaly pattern that exists after day 50 (Fig. 5). However, the substantial variability in the tropical mean latent heat flux and shortwave flux anomaly fields makes the long-term weakening of the anomalous ocean heat content nonmonotonic (Fig. 6).

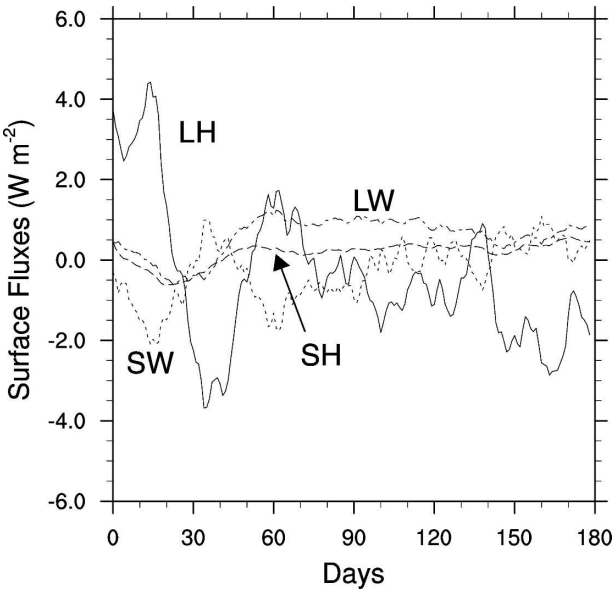

FIG. 9. Ensemble mean 30°N–30°S, 0°–360°E averaged tropical surface fluxes as a function of time after imposition of the hot spot. Positive values represent a flux of heat out of the ocean.

Some evidence exists in the composites of Waliser (1996) for suppression of latent heat fluxes across large portions of the Tropics in the month after peak amplitude of the hot spot (see his Fig. 9). However, the monthly mean composites shown in Waliser (1996) are difficult to directly compare to the higher-resolution results we show here, particularly since a monthly average may straddle portions of the transient oscillatory response containing both enhanced and suppressed periods of tropical mean latent heat flux. The Comprehensive Ocean–Atmosphere Data Set (COADS) used in Waliser (1996) also has inherent limitations in temporal and spatial coverage that may limit direct comparison to our higher-resolution flux and wind speed fields.

It should also be noted that CAM2 shortwave radiative forcing due to tropical clouds is much weaker than observed, as has been documented for previous versions of the model (e.g., Kiehl et al. 1998). These biases in shortwave cloud forcing provide a cautionary note on the results presented above, in that shortwave cloud radiative forcing is likely more important in the transient atmosphere–ocean response to a hot spot than our model indicates. This caveat should be considered when comparing our study to those that cite negative shortwave cloud feedbacks as being the primary limiting mechanism for tropical SSTs (e.g., Ramanathan

and Collins 1991). We do note, however, that Lau and Sui (1997) used observations from the Tropical Ocean Global Atmosphere Coupled Ocean–Atmosphere Response Experiment (TOGA COARE; Webster and Lukas 1992) to suggest that latent heat flux dominates west Pacific oceanic cooling during ISO-related westerly wind bursts. Westerly wind bursts generally succeed positive west Pacific SST anomalies associated with the ISO.

Figure 9 has established that latent heat flux anomalies dominate the initial tropical mean response to the hot spot in our model. At first glance, suppression of latent heat fluxes through reduced atmosphere–ocean disequilibrium, as suggested by Wallace (1992), might be the expected cause of the remote tropical warming after day 20. This mechanism has also been recently proposed as a means of forcing remote tropical SSTs during ENSO events (Chiang and Sobel 2002). Such studies hypothesize that the relatively rapid homogenization of tropical temperature after an initial tropospheric warming by convection near the warm SST anomaly leads, via convective adjustment of the remote boundary layer to the tropospheric temperature increase, to decreased air–sea humidity differences across the Tropics. These reductions in disequilibrium reduce latent heat fluxes and warm remote tropical SSTs. This mechanism does not appear to be of first-order importance in our simulations, at least in the transient oscillatory response to the hot spot (before day 60), as we will show below in our linearized model of tropical mean latent heat flux anomalies.

Latent heat flux anomalies also dominate the transient response in the vertically averaged MSE budget of the tropical atmosphere. Figure 10 shows ensemble mean anomalies in vertically averaged MSE tendency, surface latent and sensible heat fluxes, and the convergence of shortwave and longwave fluxes for the first 70 days of the simulation. MSE transport out of the tropical belt is small because our model has no appreciable background equator-to-pole temperature gradient, and thus essentially no Hadley circulation or baroclinic eddies. Thus, the transport term is not shown here. Variations in atmospheric MSE in the tropical band are clearly controlled mostly by surface latent heat flux anomalies. Longwave and shortwave cloud feedbacks in this model are relatively small in the context of variations in the tropical mean MSE budget, although we cannot rule out important localized feedbacks.

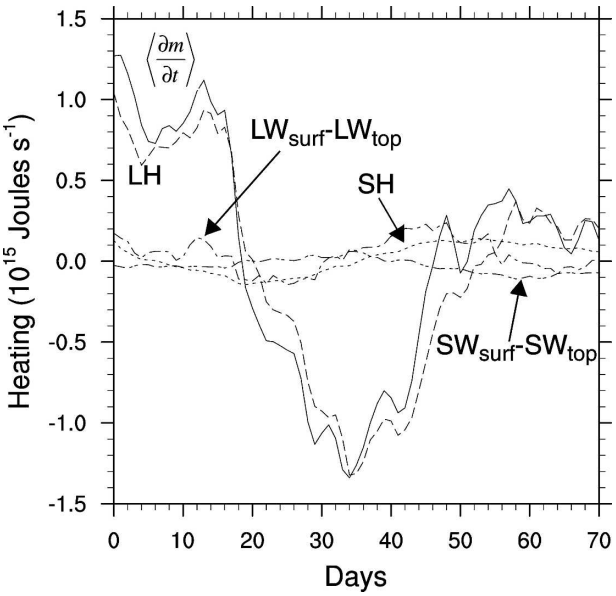

FIG. 10. Ensemble mean tropical averaged (40°N–40°S, 0°–360°E) vertically integrated atmospheric moist static energy tendency, surface latent heat flux, surface sensible heat flux, and longwave and shortwave flux divergence anomalies as a function of time after imposition of the hot spot. Anomalies are calculated relative to the climatology of the 28°C control simulation.

5. Analysis of latent heat flux

We now examine the processes responsible for the evolution of surface latent heat flux anomalies in response to the hot spot. Figure 11 shows 30°N–30°S averaged anomalies in latent heat flux and wind speed as a function of longitude for day 15 and day 40 of the simulation. Wind speed was calculated as the magnitude of the daily averaged vector wind. Day 15 and day 40 approximately correspond to the periods of peak-enhanced and suppressed tropical mean latent heat

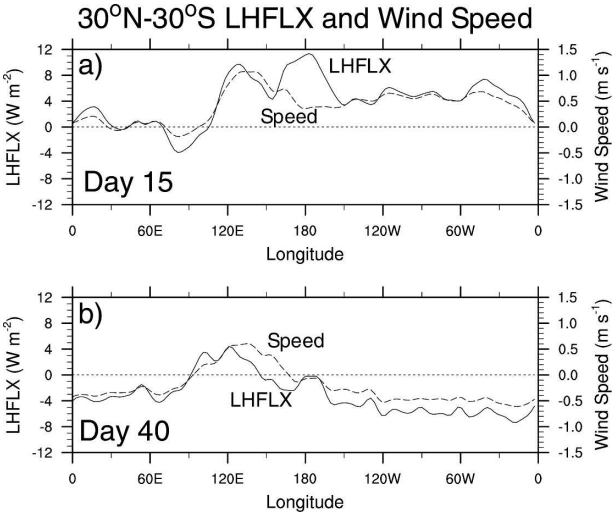

FIG. 11. Ensemble mean 30°N–30°S averaged latent heat flux and wind speed anomalies for (a) day 15 and (b) day 40 after imposition of the hot spot.

fluxes, respectively. With the possible exception of locations near the hot spot on day 15, latent heat flux anomalies generally track anomalies in wind speed. Wind speed and latent heat flux are enhanced across most of the Tropics on day 15 and suppressed across most of the Tropics on day 40. An exception on day 40 is that wind speed and latent heat flux are both enhanced within 90° to the west of the hot spot center. Weakened westerly anomalies associated with the Rossby wave response to convective heating near the hot spot appear to contribute to these enhanced wind speeds and fluxes (Fig. 3).

To confirm that wind speed anomalies are primarily responsible for the variations in tropical mean latent heat flux that we observe, we partition the latent heat flux anomaly by linearization of the bulk formula for latent heat flux,

$$\mathrm{LH}' = C[v'\overline{\Delta q} + \Delta q'\bar{v} + (\Delta q' v')'], \qquad (3)$$

where v is the wind speed in the lowest atmosphere model layer, Δq is the difference between the saturation specific humidity of the ocean surface and the specific humidity of the lowest atmosphere model level, overbars represent the climatology of the 15-yr 28°C control simulation, and primes represent the deviation from this climatology. Here C is a constant (1756 J m^{-3}) and represents the product of density, latent heat of vaporization, and the exchange coefficient for evaporation. The constant C was subjectively determined to provide the best fit to the actual tropical mean latent heat flux anomaly from the climate model. Our expression for the flux anomaly does not account for variations in stability or density that may alter C.

The linearized expression for the latent heat flux anomaly does a reasonably good job of reproducing the actual model latent heat flux anomaly (Fig. 12). The largest discrepancy occurs in the period of suppressed latent heat fluxes from days 20 to 40, where the total linearized flux anomaly underestimates the true anomaly by about 40%. We did not identify why the approximation performs relatively poorly during this period of suppressed fluxes. One possibility is that boundary layer stabilization due to the anomalously warm troposphere, accompanied by areas of cold SST, may make our assumption of constant C relatively poor during days 20–40. Because we calculate wind speed as the magnitude of the daily vector wind, strong anomalies in eddy variance due to processes on time scales of fewer than 2 days could also affect the accuracy of our calculations.

Figure 12 shows that variations in wind speed dominate tropical mean anomalies in latent heat flux within the first 60 days of the simulation. Flux anomalies due to air–sea disequilibrium are smaller than those associated with wind speed and tend to oppose the wind-driven and total flux anomalies during the first 60 days. However, anomalies in air–sea disequilibrium can be locally important for the evolution of surface flux, particularly in the vicinity of the hot spot near day 0 (not shown here). After day 60, anomalies in latent heat flux due to variations in wind speed are generally negative and highly variable. Those associated with air–sea disequilibrium are positive and relatively constant at about +1 W m^{-2}, presumably due to the heightened SST across large portions of the Tropics (Fig. 5).

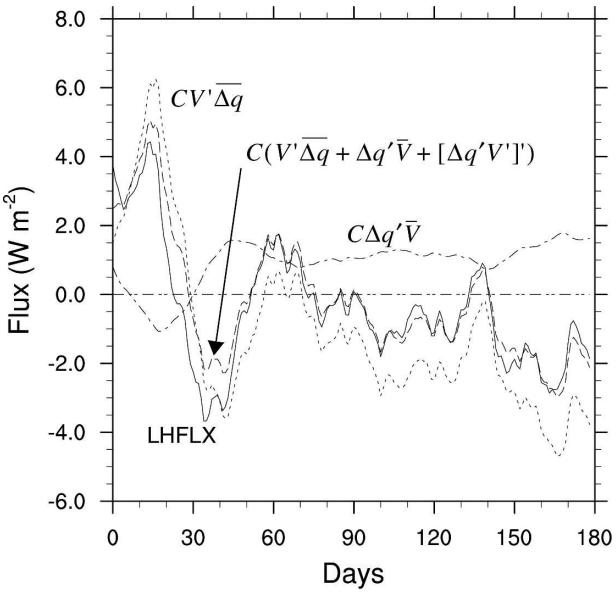

FIG. 12. Ensemble mean 30°N–30°S, 0°–360°E averaged tropical latent heat flux and linearized latent heat flux terms derived from the bulk formula, as a function of time after imposition of the hot spot. The total latent heat flux anomaly as derived from the linearized bulk formula is also shown. Positive values represent a flux of heat out of the ocean. Primes indicate a deviation from the 28°C control simulation and overbars represent the climatology of the 28°C control simulation.

The processes responsible for generating these wind-driven latent heat flux anomalies after imposition of the hot spot are not transparent. Figure 2 shows development of strong vector wind anomalies at days 10–20 of the simulation. These strong anomalies, when added to the weak easterly climatological flow (Fig. 1), would be expected to generate enhanced wind speed and thus enhanced latent heat fluxes. The anomalously high latent heat fluxes that peak near day 15 seem to confirm this behavior. However, anomalous surface easterlies occur to the east of 180° between days 30 and 40 that add constructively to the mean easterly flow. Latent heat fluxes and wind speed are suppressed in those regions (cf. Figs. 2, 3, and 11).

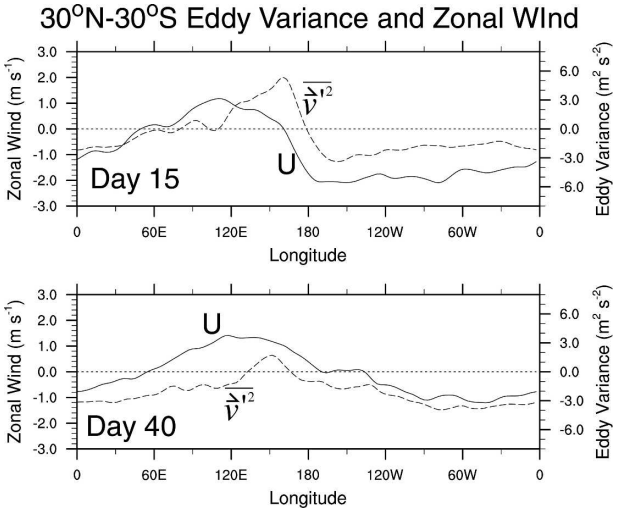

FIG. 13. Ensemble mean 30°N–30°S averaged zonal wind and eddy variance anomalies for (a) day 15 and (b) day 40 after imposition of the hot spot.

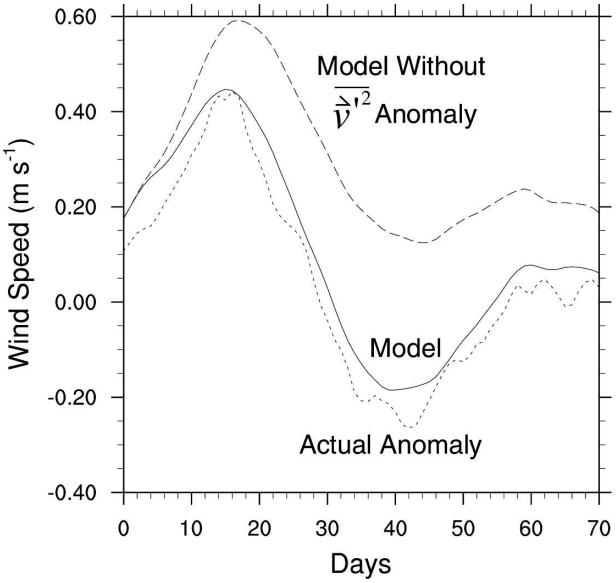

FIG. 14. Ensemble mean 30°N–30°S, 0°–360°E averaged actual wind speed anomalies, wind speed anomalies reconstructed from vector mean wind and eddy variance, and reconstructed wind speed anomalies neglecting anomalous eddy variance.

Suppressed eddy variance may help explain the suppression of wind speed that peaks around days 30–40 of the simulation. Figure 13 shows 30°N–30°S averaged ensemble mean anomalies in eddy variance and zonal wind for day 15 and day 40. Eddy wind components are defined as anomalies from the running 10-day-averaged wind components (as described in the appendix), effectively corresponding to a 20-day high-pass filter. Eddy variance is suppressed over large portion of the Tropics during both day 15 and day 40, with this suppression largely occurring in regions of easterly anomalies to the east of the hot spot. At day 15, easterly zonal wind anomalies are on the order of -2 m s^{-1}, which appears to swamp the influence of suppressed eddy variance anomalies in determining wind speed. However, although eddy suppression of similar amplitude occurs at day 40, easterly zonal wind anomalies are now weaker and average only about -1 m s^{-1}, decreasing their influence on the total wind speed anomaly.

To determine the relative importance of eddy variance anomalies to wind speed anomalies, we do an approximate reconstruction of the tropical mean wind speed anomaly using vector mean and eddy components. This method is described in the appendix. The approximation does a reasonable job of reproducing the actual tropical mean wind speed anomaly up to day 70, as shown in Fig. 14. When we neglect the anomalous part of the eddy variance field (relative to the 28°C control simulation), our analysis indicates that ensemble mean tropical wind speed should be enhanced within the entire first 70 days of the simulation. Recall that vector wind anomalies on day 40 to the east of 180° (Figs. 2 and 13), when added to the climatological flow (Fig. 1), would suggest an enhancement of vector mean wind. Wind speed anomalies are clearly negative in this region (Fig. 11), and the analysis of Fig. 14 indicates that the suppression in wind speed during days 30–50 appears to be forced by the suppression of eddy variance.

What do the dominant eddies in the model look like? To determine this, we did a lag regression of eddy wind components and eddy vorticity from the 15-yr 28°C control simulation onto eddy vorticity at 20°N, 180°. Here 20°N is near the latitude of the highest average eddy vorticity variance. The dominant eddies resemble tropical depression (TD)-type disturbances of the tropical atmosphere (e.g., Takayabu and Nitta 1993), having wavelengths of about 4000 km, northwest propagation at about 5 m s^{-1}, and a southwest–northeast tilt with latitude (Fig. 15). Given the northeast–southwest tilt of these eddies, they would be expected to lose energy to the mean flow through barotropic conversion in regions of anticyclonic shear of the zonal wind (e.g., Lau and Lau 1992). During periods of enhanced low-level easterly equatorial flow, such anticyclonic shear is enhanced near 15°–20° latitude (e.g., Fig. 2). Precipitation also tends to be weakly suppressed in these regions of enhanced anticyclonic shear (e.g., Fig. 2, day 20), and a potential diabatic heat source for these synoptic-scale disturbances may also be suppressed (e.g., Shapiro 1986).

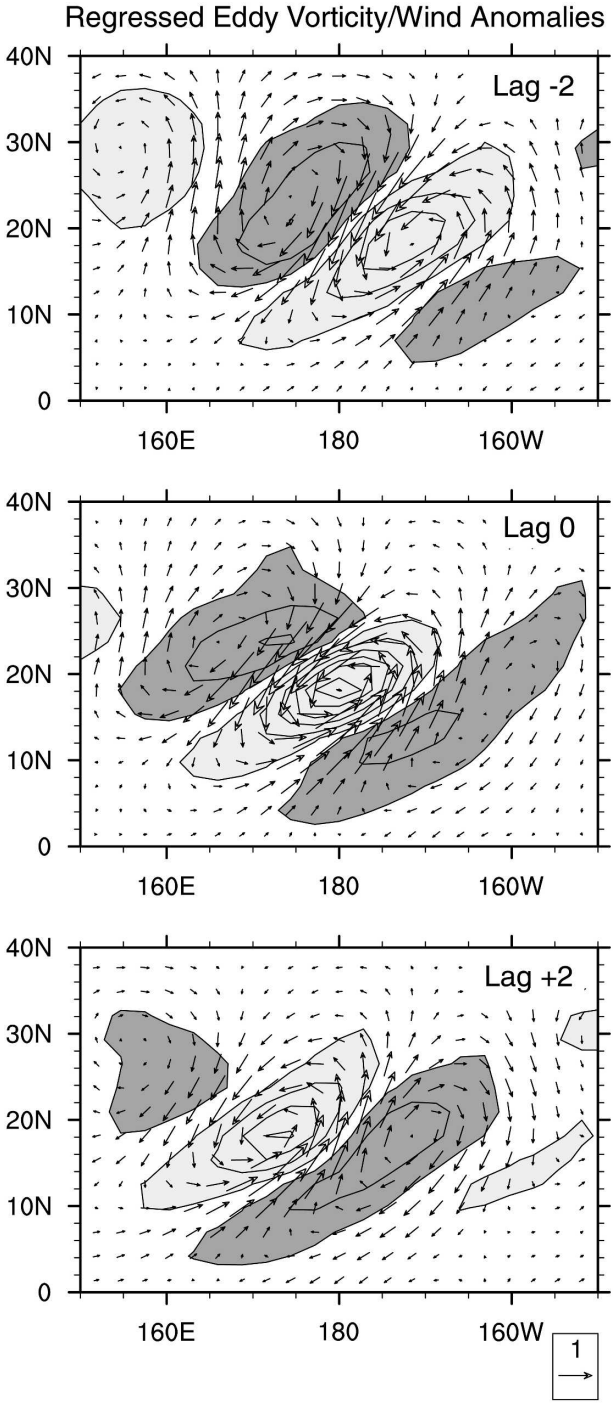

FIG. 15. Eddy 850-hPa wind and vorticity anomalies regressed onto 20°N, 180° eddy vorticity as a function of lag in days. The reference wind vector (m s^{-1}) is shown at the bottom right. The vorticity contour interval is 1.4×10^{-6} s^{-1}, starting at 0.7×10^{-6} s^{-1}. Values greater (less) than 0.7×10^{-6} s^{-1} (-0.7×10^{-6} s^{-1}) are light (dark) shaded.

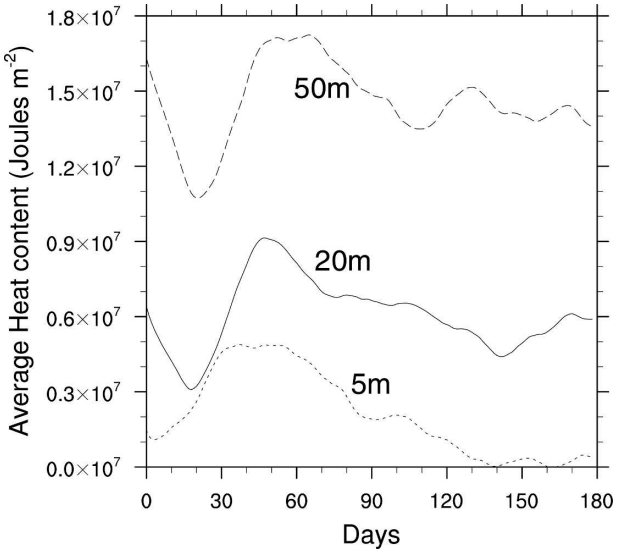

FIG. 16. Ensemble mean 30°N–30°S, 0°–360°E averaged tropical oceanic heat content as a function of time after imposition of the hot spot for SOM depths of 50 (dashed), 20 (solid), and 5 (dotted) m.

Synoptic-scale eddies have been observed to be suppressed in association with lower-tropospheric easterly wind anomalies associated with the ISO (Maloney and Dickinson 2003). Maloney and Esbensen (2007) showed using Quick Scatterometer (QuikSCAT) ocean vector winds that suppression of synoptic-scale eddies contributes importantly to the negative wind speed and latent heat flux anomalies over the east Pacific warm pool during ISO easterly periods. Our modeling results indicating eddy suppression during periods of anomalous low-level easterly flow and the resulting wind speed suppression are consistent with these observational results.

6. Sensitivity tests

The 20-m SOM depth we use above is a reasonable mean depth for the mixed layer in the west Pacific warm pool, one of the centers of maximum convective activity and SST variability for the ISO. Experiments using 5- and 50-m slab oceans demonstrate that while the response to the hot spot resembles that with the 20-m SOM, the time scale of the transient oscillation in ocean heat content decreases with decreasing SOM depth (Fig. 16). Little initial cooling is evident in the tropical mean response for the 5-m SOM ensemble simply because the hot spot is initially of low heat content and quickly damps. The anomalous heat content of the Tropics is also more rapidly damped in the 5-m ensemble than the other two ensembles and reaches zero by about day 140 of the simulation. Enhanced longwave

emission is the dominant term in this longer time-scale damped response.

Sensitivity to model basic state is briefly noted here. Imposition of a west Pacific hot spot in an experiment with a 20-m SOM using realistic February SST, radiative forcing, and continents produces behavior qualitatively similar to that in the idealized experiments (not shown). A relative minimum in oceanic heat content occurs at about day 30, followed by a recovery by days 50–60. The time scale of the oscillatory transient response appears to be a bit longer than in our idealized 20-m SOM case. Air–sea exchange is dominated by latent heat flux, as in our idealized case (not shown here). However, in this perpetual February experiment a 15-member ensemble is not sufficient to produce a statistically significant oscillation in tropical ocean heat content. The lack of statistical significance with a small ensemble using a realistic background is consistent with the findings of Toyoda et al. (1999) and Nakajima et al. (2004), who imposed hot spots on a basic state with realistic equator-to-pole SST gradient. In their experiments, a 64–128-member ensemble appeared to be necessary to identify with confidence the salient response to a hot spot above the background noise.

7. Conclusions and discussion

An idealized experiment with a GCM coupled to a slab ocean model (SOM) is conducted to examine the response of the tropical atmosphere–ocean system to the switch-on of an equatorial +2°C SST hot spot anomaly. A spatially uniform aquaplanet with 28°C SST is the background state on which the hot spot is imposed. A 15-member ensemble is generated for the hot spot experiment using random initial conditions taken from a 15-yr control simulation with fixed globally uniform 28°C SSTs.

The response to a +2°C hot spot using a 20-m SOM is examined. Strong convective anomalies develop in the vicinity of the hot spot that reach their peak amplitude near day 10. These convective anomalies force an anomalous large-scale circulation that resembles the response to a steady equatorial heat source described by Gill (1980). This circulation is accompanied by positive tropical mean tropospheric temperature anomalies that peak around day 20. Day 20 also corresponds to a relative minimum in tropical ocean heat content, caused primarily by loss of oceanic heat through enhanced latent heat fluxes in the vicinity of the hot spot. In this particular model, shortwave cloud forcing is weaker than observed, and so latent heat flux variability dominates the transient response to the hot spot in the surface energy budget.

After day 20, tropical mean latent heat fluxes are suppressed across the remote Tropics, and the remote tropical ocean warms as a result. Suppressed latent heat fluxes peak near day 40 and produce a maximum in ocean heat content about day 50. The anomalous heat content of the tropical oceans at day 50 is greater than at day 0. The exchange of heat between the ocean and atmosphere in response to the hot spot results in a statistically significant oscillation in tropical mean ocean heat content with a time scale of about 70 days. A corresponding out-of-phase oscillation in vertically integrated atmospheric moist static energy accompanies this oscillation in ocean heat content. A local unforced oscillation in sea surface temperature and precipitation is not locally generated near the hot spot, and analysis of the MSE budget suggests that this is consistent with the theoretical results of Sobel and Gildor (2003), as parameters inferred from the budgets appear to place the present model in a stable regime according to their analysis. After day 70, the positive heat content anomalies that are distributed across the tropical oceans decay slowly in time, accompanied by an anomalous upward longwave flux from the ocean surface.

Latent heat flux variability regulates the oscillatory response to the hot spot and redistribution of heat to the remote Tropics and is primarily wind driven. Latent heat flux anomalies before day 20 are dominated by the vector mean component of the wind, and the suppression of latent heat flux between day 20 and day 50 results primarily from suppression of eddy wind variance. The dominant eddies in the model resemble tropical depression–type disturbances of the observed atmosphere. Regions of anomalous low-level easterly flow are associated with a suppression of synoptic-scale wind variability in the model that leads to a decrease in wind speed and produces negative latent heat flux anomalies.

Our results have implications for the short-term regulation of sea surface temperatures and lead to a hypothesis that is testable in principle. The results suggest that the response of the large-scale circulation to a localized oceanic hot spot can modulate sea surface temperatures over a broader region, through the impact of the induced surface winds on the surface latent heat flux. The results further suggest that higher-frequency components of the climate system, including tropical synoptic-scale disturbances, contribute to this response by modulating the surface wind speed and associated latent heat flux variability. In particular, synoptic-scale eddy suppression during periods of low-level equatorial easterly anomalies may contribute to warming the remote tropical ocean away from the hot spot. As demonstrated in Gill (1980) and other studies, an

extensive region of low-level tropical easterly anomalies can be forced by convective heating near the hot spot. If this reduces transient activity and thus mean surface wind speed, it should lead to SST warming. This behavior, if strong enough to be significant, might be detectable in observations, though the finite length of the observational record and the higher level of noise in the real atmosphere than in our aquaplanet simulations may make such detection difficult.

We note several caveats to this study. First, the NCAR CAM2 we use is characterized by relatively weak tropical shortwave cloud forcing as compared to observations (e.g., Kiehl and Gent 2004). Thus, shortwave cloud feedbacks are likely underestimated in our simulations.

Second, while a statistically significant oscillatory response in ocean heat content was obtained in our idealized experiment, an additional experiment with a 15-member ensemble in which a west Pacific hot spot was imposed on a realistic distribution of SSTs and continents produced a response that was qualitatively similar but not statistically significant. This result was foreshadowed by the work of Toyoda et al. (1999), who found that a 64–128-member ensemble was necessary to determine the salient features of the hot spot response in an aquaplanet simulation with a realistic equator-to-pole temperature gradient.

A third caveat is that the ocean may produce a dynamical response that modulates the SST response to the hot spot. West Pacific hot spots often form in association with shallow oceanic mixed layers that deepen rapidly in the SST cooling phase associated with enhanced convection and westerly wind bursts (Anderson et al. 1996). This deepening of the mixed layer during the cooling phase through turbulent mixing can modulate the thermal response of the ocean to surface flux forcing, although the reduction of shortwave penetration through the base of the mixed layer may play a partly opposing role, reducing the importance of this process (Gildor and Sobel 2007, manuscript submitted to *J. Climate*). Ocean advection associated with the formation of a Yoshida jet caused by strong westerly wind stresses can also be an important regulator of SST in particular cases (e.g., Cronin et al. 2000). Our simple SOM of uniform mixed layer depth cannot account for these dynamical processes.

Acknowledgments. We thank Masahiro Sugiyama and one anonymous reviewer for their insightful reviews of the original manuscript. This work was supported by the Climate Dynamics Program of the National Science Foundation (NSF) under Grants ATM-0327460 and ATM-0632341 (EDM). This research was also prepared by EDM and funded under Award NA05OAR4310006 from the National Oceanic and Atmospheric Administration (NOAA), U.S. Department of Commerce. The statements, findings, conclusions, and recommendations do not necessarily reflect the views of NSF, NOAA, or the Department of Commerce. Supercomputing resources were provided by the National Center for Atmospheric Research, Boulder, Colorado.

APPENDIX

Partitioning of Wind Speed

We approximate the wind speed anomaly in the hot spot experiments by first decomposing wind components into their 10-day running average and the deviation from this 10-day average. We refer to these deviations as the eddy component. Using the u component of wind as an example, we can write this decomposition as follows:

$$u = \overline{u} + u'. \tag{A1}$$

The wind speed anomaly relative to the 15-yr climatology of the 28°C control simulation can thus be approximated by

$$s''_{\text{total}} = \sqrt{\overline{u}^2 + \overline{v}^2 + \overline{u'^2} + \overline{v'^2}} - \left[\sqrt{\overline{u}^2 + \overline{v}^2 + \overline{u'^2} + \overline{v'^2}}\,\right], \tag{A2}$$

where the brackets represent an average over the 15-yr 28°C control simulation. The eddy variance components can be further decomposed into a climatological component, and a deviation from this climatological component:

$$\overline{u'^2} = [\overline{u'^2}] + (\overline{u'^2})''. \tag{A3}$$

We can recompute the wind speed anomaly but now neglecting the portion of the eddy variance that differs from the 28°C control simulation:

$$s''_{\text{vector}} = \sqrt{\overline{u}^2 + \overline{v}^2 + [\overline{u'^2}] + [\overline{v'^2}]} - \left[\sqrt{\overline{u}^2 + \overline{v}^2 + \overline{u'^2} + \overline{v'^2}}\,\right]. \tag{A4}$$

The effective wind speed anomaly in (A4) should now only be attributable to 10-day-averaged vector winds.

REFERENCES

Anderson, S. P., R. A. Weller, and R. Lukas, 1996: Surface buoyancy forcing and the mixed layer of the western Pacific warm pool: Observations and 1D model results. *J. Climate,* **9,** 3056–3085.

Bantzer, C. H., and J. M. Wallace, 1996: Intraseasonal variability in tropical mean temperature and precipitation and their relation to the tropical 40–50 day oscillation. *J. Atmos. Sci.,* **53,** 3032–3045.

Barsugli, J., S.-I. Shin, and P. D. Sardeshmukh, 2005: Tropical climate regimes and global climate sensitivity in a simple setting. *J. Atmos. Sci.,* **62,** 1226–1240.

Bretherton, C. S., and A. H. Sobel, 2002: A simple model of a convectively coupled Walker circulation using the weak temperature gradient approximation. *J. Climate,* **15,** 2907–2920.

——, P. N. Blossey, and M. Khairoutdinov, 2005: An energy-balance analysis of deep convective self-aggregation above uniform SST. *J. Atmos. Sci.,* **62,** 4273–4292.

Chiang, J. C. H., and A. H. Sobel, 2002: Tropical tropospheric temperature variations caused by ENSO and their influence on the remote tropical climate. *J. Climate,* **15,** 2616–2631.

Clement, A. C., R. Seager, M. A. Cane, and S. E. Zebiak, 1996: An ocean dynamical thermostat. *J. Climate,* **9,** 2190–2196.

——, ——, and R. Murtugudde, 2005: Why are there tropical warm pools. *J. Climate,* **18,** 5294–5311.

Cronin, M. F., M. J. McPhaden, and R. H. Weisberg, 2000: Wind-forced reversing jets in the western equatorial Pacific. *J. Phys. Oceanogr.,* **30,** 657–676.

Gildor, H., and A. H. Sobel, 2007: The role of ocean mixed layer dynamics in the atmospheric intraseasonal oscillation. *J. Climate,* submitted.

Gill, A. E., 1980: Some simple solutions for the heat-induced tropical circulation. *Quart. J. Roy. Meteor. Soc.,* **106,** 447–462.

Hansen, J., A. Lacis, D. Rind, G. Russell, P. Stone, I. Fung, R. Ruedy, and J. Lerner, 1984: Climate sensitivity: Analysis of feedback mechanisms in climate processes and sensitivity. *Climate Processes and Climate Sensitivity, Geophys. Monogr*., Vol. 29, Amer. Geophys. Union, 130–163.

Hartmann, D. L., and M. L. Michelsen, 1993: Large-scale effects on the regulation of tropical sea surface temperature. *J. Climate,* **6,** 2049–2062.

Heckley, W. A., and A. E. Gill, 1984: Some simple analytical solutions to the problems of forced equatorial long waves. *Quart. J. Roy. Meteor. Soc.,* **110,** 203–217.

Hosaka, M., M. Ishiwatari, S.-I. Takehiro, K. Nakajima, and Y.-Y. Hayashi, 1998: Tropical precipitation patterns in response to a local warm SST area placed at the equator of an aqua planet. *J. Meteor. Soc. Japan,* **76,** 289–305.

Kessler, W. S., 2005: The oceans. *Intraseasonal Variability in the Atmosphere–Ocean Climate System,* W. K. M. Lau and D. E. Waliser, Eds., Springer-Verlag, 175–212.

Kiehl, J. T., and P. R. Gent, 2004: The Community Climate System Model, version 2. *J. Climate,* **17,** 3666–3682.

——, J. J. Hack, and J. W. Hurrell, 1998: The energy budget of the NCAR Community Climate Model: CCM3. *J. Climate,* **11,** 1151–1178.

Kirtman, B. P., and E. K. Schneider, 2000: A spontaneously generated tropical atmospheric circulation. *J. Atmos. Sci.,* **57,** 2080–2093.

Larson, K., D. L. Hartmann, and S. A. Klein, 1999: The role of clouds, water vapor, circulation, and boundary layer structure in the sensitivity of the tropical climate. *J. Climate,* **12,** 2359–2374.

Lau, K.-H., and N.-C. Lau, 1992: The energetics and propagation dynamics of tropical summertime synoptic-scale disturbances. *Mon. Wea. Rev.,* **120,** 2523–2539.

Lau, K.-M., and C.-H. Sui, 1997: Mechanisms of short-term sea surface temperature regulation: Observations during TOGA COARE. *J. Climate,* **10,** 465–472.

——, ——, M.-D. Chao, and W.-K. Tau, 1994: An inquiry into the cirrus-cloud thermostat effect for tropical sea surface temperature. *Geophys. Res. Lett.,* **21,** 1157–1160.

Lukas, R., and E. Lindstrom, 1991: The mixed layer of the western equatorial Pacific Ocean. *J. Geophys. Res.,* **96** (Suppl.), 3343–3357.

Madden, R., and P. R. Julian, 2005: Historical perspective. *Intraseasonal Variability in the Atmosphere–Ocean Climate System,* K. M. Lau and D. E. Waliser, Eds., Springer-Verlag, 1–18.

Maloney, E. D., and D. L. Hartmann, 2001: The sensitivity of intraseasonal variability in the NCAR CCM3 to changes in convective parameterization. *J. Climate,* **14,** 2015–2034.

——, and M. J. Dickinson, 2003: The intraseasonal oscillation and the energetics of summertime tropical western North Pacific synoptic-scale disturbances. *J. Atmos. Sci.,* **60,** 2153–2168.

——, and A. H. Sobel, 2004: Surface fluxes and ocean coupling in the tropical intraseasonal oscillation. *J. Climate,* **17,** 4368–4386.

——, and S. K. Esbensen, 2005: A modeling study of summertime east Pacific wind-induced ocean–atmosphere exchange in the intraseasonal oscillation. *J. Climate,* **18,** 568–584.

——, and ——, 2007: Satellite and buoy observations of boreal summer intraseasonal variability in the tropical northeast Pacific. *Mon. Wea. Rev.,* **135,** 3–19.

Milliff, R. F., and R. A. Madden, 1996: The existence and vertical structure of fast, eastward-moving disturbances in the equatorial troposphere. *J. Atmos. Sci.,* **53,** 586–597.

Moorthi, S., and M. J. Suarez, 1992: Relaxed Arakawa–Schubert: A parameterization of moist convection for general circulation models. *Mon. Wea. Rev.,* **120,** 978–1002.

Nakajima, K., E. Toyoda, M. Ishiwatari, S.-I. Takehiro, and Y.-Y. Hayashi, 2004: Initial development of tropical precipitation patterns in response to a local warm SST area: An aqua-planet ensemble study. *J. Meteor. Soc. Japan,* **82,** 1483–1504.

Neale, R. B., and B. J. Hoskins, 2000a: A standard test for AGCMs including their physical parameterizations. I: The proposal. *Atmos. Sci. Lett.,* **1,** 101–107.

——, and ——, 2000b: A standard test for AGCMs including their physical parameterizations. II: Results for the Met Office model. *Atmos. Sci. Lett.,* **1,** 108–114.

Pierrehumbert, R. T., 1995: Thermostats, radiator fins, and the local runaway greenhouse. *J. Atmos. Sci.,* **52,** 1784–1806.

Ralph, E. A., K. Bi, and P. P. Niiler, 1997: A Lagrangian description of the western equatorial Pacific response to the wind burst of December 1992. *J. Climate,* **10,** 1706–1721.

Ramanathan, V., and W. Collins, 1991: Thermodynamic regulation of ocean warming by cirrus clouds deduced from observations of the 1987 El Niño. *Nature,* **351,** 27–32.

Seager, R., and R. Murtugudde, 1997: Ocean dynamics, thermocline adjustment, and regulation of tropical Pacific SST. *J. Climate,* **10,** 521–534.

Shapiro, L. J., 1986: The three-dimensional structure of synoptic-scale disturbances over the tropical Atlantic. *Mon. Wea. Rev.,* **114,** 1876–1891.

Shinoda, T., and H. H. Hendon, 1998: Mixed layer modeling of intraseasonal variability in the tropical western Pacific and Indian Oceans. *J. Climate,* **11,** 2668–2685.

Sobel, A. H., and H. Gildor, 2003: A simple time-dependent model of SST hot spots. *J. Climate,* **16,** 3978–3992.

——, C. S. Bretherton, H. Gildor, and M. Peters, 2004: Con-

vection, cloud-radiative feedbacks and thermodynamic ocean coupling in simple models of the Walker circulation. *Earth's Climate: The Ocean–Atmosphere Interaction, Geophys. Monogr.,* Vol. 147, Amer. Geophys. Union, 393–405.

Su, H., and J. D. Neelin, 2002: Teleconnection mechanisms for tropical Pacific descent anomalies during El Niño. *J. Atmos. Sci.,* **59,** 2682–2700.

——, ——, and J. E. Meyerson, 2005: Mechanisms for lagged atmospheric response to ENSO SST forcing. *J. Climate,* **18,** 4195–4215.

Sud, Y. C., G. K. Walker, and K.-M. Lau, 1999: Mechanisms regulating sea-surface temperatures and deep convection in the Tropics. *Geophys. Res. Lett.,* **26,** 1019–1022.

Sun, D.-Z., and Z. Liu, 1996: Dynamic ocean–atmosphere coupling: A thermostat for the Tropics. *Science,* **272,** 1148–1150.

Takayabu, Y. N., and T. Nitta, 1993: 3-5 day period disturbances coupled with convection over the tropical Pacific Ocean. *J. Meteor. Soc. Japan,* **71,** 221–246.

Toyoda, E., K. Nakajima, M. Ishiwatari, and Y.-Y. Hayashi, 1999: Response of the tropical atmosphere to a localized warm SST area: Time-development observed in an aqua-planet ensemble experiment. *Nagare Multimedia 99,* Vol. 18. [Available online at http://www.nagare.or.jp/mm/99/toyoda.]

Waliser, D. E., 1996: Formation and limiting mechanisms for very high sea surface temperature: Linking the dynamics and thermodynamics. *J. Climate,* **9,** 161–188.

——, and N. E. Graham, 1993: Convective cloud systems and warm pool SSTs: Coupled interactions and self-regulation. *J. Geophys. Res.,* **98,** 12 881–12 893.

——, K. M. Lau, and J.-H. Kim, 1999: The influence of coupled sea surface temperatures on the Madden–Julian oscillation: A model perturbation experiment. *J. Atmos. Sci.,* **56,** 333–358.

Wallace, J. M., 1992: Effect of deep convection on the regulation of tropical sea surface temperature. *Nature,* **357,** 230–231.

Wang, B., and X. Xie, 1998: Coupled modes of the warm pool climate system. Part I: The role of air–sea interaction in maintaining Madden–Julian oscillation. *J. Climate,* **11,** 2116–2135.

Webster, P. J., and R. Lukas, 1992: TOGA COARE: The Coupled Ocean–Atmosphere Response Experiment. *Bull. Amer. Meteor. Soc.,* **73,** 1377–1416.

Weller, R. A., and S. P. Anderson, 1996: Surface meteorology and air–sea fluxes in the western equatorial Pacific warm pool during the TOGA Coupled Ocean–Atmosphere Response Experiment. *J. Climate,* **9,** 1959–1990.

Wheeler, M., and G. N. Kiladis, 1999: Convectively coupled equatorial waves: Analysis of clouds and temperature in the wavenumber–frequency domain. *J. Atmos. Sci.,* **56,** 374–399.

Zhang, C., M. Dong, S. Gualdi, H. H. Hendon, E. D. Maloney, A. Marshall, K. R. Sperber, and W. Wang, 2006: Simulations of the Madden–Julian oscillation in four pairs of coupled and uncoupled global models. *Climate Dyn.,* **27,** 573–592.

Zhang, G. J., and N. A. McFarlane, 1995: Sensitivity of climate simulations to the parameterization of cumulus convection in the Canadian Climate Centre General Circulation Model. *Atmos.–Ocean,* **33,** 407–446.

——, and M. J. McPhaden, 1995: The relationship between sea surface temperature and latent heat flux in the equatorial Pacific. *J. Climate,* **8,** 589–605.

Zhang, M. H., R. D. Cess, and S. C. Xie, 1996: Relationship between cloud radiative forcing and sea surface temperatures over the entire tropical oceans. *J. Climate,* **9,** 1374–1384.